SOLUTION OF THE NAVIER STOKES EQUATIONS FOR AEROFOILS UNDERGOING COMBINED TRANSLATION PITCH OSCILLATIONS

Scott Shaw and Ning Qin

Cranfield College of Aeronautics,
United Kingdom

Abstract

The aerodynamics of aerofoils performing unsteady motions is important for the design of helicopter rotors. In this paper numerical solutions of the Reynolds averaged Navier-Stokes equations are used to investigate the flowfield around an aerofoil performing combined translation-pitch oscillations. Computed results are compared with suitable experimental data for a NACA 0012 aerofoil undergoing both inplane and pitching oscillations in transonic flow, generally reasonable agreement is found between the computations and experiment. In addition the results of calculations performed for combined translation-pitching aerofoils are compared with those obtained for the individual motions.

Introduction

The prediction of the aerodynamic phenomena associated with helicopters in forward flight presents a significant challenge for computational fluid dynamics. The rotor flowfield is one which is dominated by unsteady effects arising principally as a result of the complex time dependent motion of the rotor blades. Despite significant advances over the last decade the routine solution of the Reynolds averaged Navier-Stokes equations for problems of this level of complexity is beyond the current capability of computational fluid dynamics. In order to achieve a better understanding of the dominant physical processes it is reasonable to study the aerodynamics of aerofoils which undergo representative motions. In this respect the aerodynamic performance of aerofoils undergoing inplane and pitching oscillations are of particular interest.

In forward flight the motion of the rotor blade in the plane of the rotor disc can be represented by longitudinal oscillations. Maresca, Favier and Rebout[1] and Gursul, Ho and Lin[2,3,4,5] investigated the influence of relatively low amplitude longitudinal oscillations at fixed angles of incidence. In general only weak unsteady effects were observed for angles of incidence below the static stall but when the static stall angle of attack was exceeded dynamic stall phenomena usually associated with pitching aerofoils were observed. For larger amplitude longitudinal oscillations Krause and Schweitzer[6] have demonstrated that inplane motions can play an important role in the development of the flowfield for angles of attack below that of static stall. Morinishi and Muratu[7] have presented solutions of the incompressible Navier-Stokes equations for oscillating aerofoils at high angles of attack in laminar flow.

The experimental investigations mentioned above have mainly demonstrated the influence of inplane oscillations at very low free stream Mach numbers and high angle of attacks. To the authors' knowledge no detailed investigations have been carried out for the corresponding motion in the transonic flow regime.

Solutions of the Euler equations for a NACA 0012 aerofoil undergoing inplane oscillations representative of helicopter forward flight were presented by Lerat and Sides[8] for compressible flow conditions. Their calculations showed good agreement with three dimensional rotor test data. Habibie, Laschka and Weishaupl[9] and Lin and Pahlke[10] have also presented solutions of the Euler equations for inplane oscillations.

The use of the Euler equations to model helicopter rotors in high speed forward flight is questionable due to the increasing importance of shock-boundary layer interactions in the development of the unsteady flowfield as the helicopter rotor approaches its maximum advance ratio. Shaw and Qin[11] have recently presented the results of calculations performed using the thin layer Navier-Stokes equations together with the Baldwin-Lomax turbulence model. Comparison of the computed results with three dimensional experimental data is generally good provided that the shock-boundary layer interactions do not cause large scale separations.

The aerodynamics of aerofoils in pitch have received considerable attention due to the importance of such motions in aeroelastics and dynamic stall. Calculated results obtained using the Euler equations for standard AGARD test cases have been presented by Gaitonde[12], Badcock[13], Richter and Leyland[14] and Paraschivoiu[15]. The calculated results show a high level of consistency when compared with one another but generally only fair agreement is found when comparison is made with experiment.

The investigation of combined translation-pitch oscillations has largely been confined to incompressible

flow. Favier et al[16,17] have presented experimental measurements for a NACA 0012 aerofoil. For moderate reduced frequencies and amplitudes velocity variations were found to be dominant when the fluctuations were in phase, while for out of phase motions incidence variations dominated the development of the flow. For angles of attack through and beyond the static stall angle of attack the influence of coupling incidence and velocity fluctuations was found to be more complex.

The use of analytical methods to predict the influence of combined pitching and translation oscillations was reviewed by Van der Wall and Leischman[18]. Expressions for the lift transfer function were obtained for incompressible flow which show good agreement with low Mach number Euler calculations. Numerical results obtained using the Navier-Stokes equations have been presented by Pascazio et al[19] which capture the salient features of the unsteady flowfield.

In the present work a finite volume method based upon Oshers flux difference splitting is used to solve the compressible thin layer Navier-Stokes equations for the transonic flow around aerofoils undergoing in-plane and pitching oscillations. The method has been used to study the unsteady aerodynamics of a NACA 0012 aerofoil at flow conditions representative of the high speed forward flight of helicopter rotors. Results of calculations performed for a NACA 0012 aerofoil undergoing inplane and pitching oscillations are compared with experimental measurements. In addition the results of combined translation-pitch oscillations are compared with the individual motions.

Governing Equations

The Navier-Stokes equations express the conservation of mass, momentum and energy and may be written for curvilinear co-ordinates as,

$$\frac{\partial Q}{\partial t}+\frac{\partial(E_i-E_v)}{\partial \xi}+\frac{\partial(F_i-F_v)}{\partial \eta}=0 \qquad (1)$$

in which Q is the vector of conserved variables, E_i and F_i are the convective flux vectors and E_v and F_v are the viscous flux vectors in the ξ and η directions respectively.

In the current work the thin layer form of the Navier-Stokes equations are solved. Under the thin layer approximation derivatives in the tangential direction are neglected in the viscous flux terms. The viscous flux vector in the ξ-direction is neglected and the remaining terms in Equation (1) are given by,

$$E_i=\begin{pmatrix}\rho U\\ \rho uU+\xi_x P\\ \rho vU+\xi_y P\\ U(e+P)\end{pmatrix}, F_i=\begin{pmatrix}\rho V\\ \rho uV+\eta_x P\\ \rho vV+\eta_y P\\ V(e+P)\end{pmatrix} \qquad (2a)$$

$$F_v=\frac{1}{Re}\begin{pmatrix}0\\ \mu a_1 u_\eta+\frac{\mu}{3}\eta_x a_2\\ \mu a_1 v_\eta+\frac{\mu}{3}\eta_y a_2\\ \mu a_1 a_3+\frac{\mu}{3}a_2\left(\eta_x u+\eta_y v\right)\end{pmatrix} \qquad (2b)$$

here,

$$a_1=\eta_x^2+\eta_y^2$$
$$a_2=\xi_x^2+\xi_y^2$$
$$a_3=\frac{u^2+v^2}{2}+\frac{c_\eta^2}{Pr(\gamma-1)}$$

and ρ, u, v, P, c, Re, Pr are density, Cartesian components of velocity, pressure, speed of sound, Reynolds number and Prandtl number respectively. U and V are the contravariant velocities calculated from,

$$U=\xi_x u+\xi_y v$$
$$V=\eta_x u+\eta_y v \qquad (2c)$$

In order to represent the effects of oscillations in both translation and pitch Equation (1) is extended for arbitrarily moving bodies in the following manner. Consider the one dimensional continuity equation,

$$\frac{\partial \rho}{\partial t}+\frac{\partial(\rho u)}{\partial x}=0 \qquad (3)$$

Integrating for a control volume whose boundaries move over time we obtain,

$$\int_{x(t_1)}^{x(t_2)}\frac{\partial \rho}{\partial t}dx+\int_{x(t_1)}^{x(t_2)}\frac{\partial(\rho u)}{\partial x}dx=0 \qquad (4)$$

After differentiation of the first term with respect to time and some further manipulation Equation (4) may be rewritten in the following form,

$$\frac{d}{dt}\int_{x(t_1)}^{x(t_2)}\rho dx+\int_{x(t_1)}^{x(t_2)}\frac{\partial}{\partial x}\rho\left(u-\frac{dx}{dt}\right)dx=0 \qquad (5)$$

in which $\frac{dx}{dt}$ is the velocity with which the control volume surface moves, referred to as the grid velocity. Similar results follow for the momentum and energy equations.

The governing equations may therefore be rewritten for arbitrarily moving bodies by replacing the velocity in the convective flux terms (Equations (2a)) with the relative velocity of the fluid with respect to the moving grid. The convective flux vectors become,

$$E_i = \begin{pmatrix} \rho U \\ \rho u U + \xi_x P \\ \rho v U + \xi_y P \\ U(e+P) + \xi_t P \end{pmatrix} \qquad F_i = \begin{pmatrix} \rho V \\ \rho u V + \eta_x P \\ \rho v V + \eta_y P \\ V(e+P) + \eta_t P \end{pmatrix} \tag{6a}$$

in which the contravariant velocities are now calculated from,

$$U = \xi_x\left(u - \frac{dx}{dt}\right) + \xi_y\left(v - \frac{dy}{dt}\right)$$
$$V = \eta_x\left(u - \frac{dx}{dt}\right) + \eta_y\left(v - \frac{dy}{dt}\right) \tag{6b}$$

Numerical procedure

Osher's flux difference splitting method is employed for the spatial discretisation of the convective flux terms, Equations (6a). Higher order spatial accuracy is obtained using MUSCL interpolation together with a flux limiter. The viscous terms are discretised using central differences. The algebraic turbulence model proposed by Baldwin and Lomax is used to provide a turbulent contribution to the viscosity.

After spatial discretisation the governing equations are reduced to a system of ordinary differential equations which are integrated in time using a first order Euler implicit scheme. One implicit step of the method can be written as,

$$\left[I + \frac{\partial E_i}{\partial Q} + \frac{\partial F_i}{\partial Q} + \frac{\partial F_v}{\partial Q}\right]\frac{\partial Q}{\partial t} = -\Delta t\left(\frac{\partial E_i}{\partial \xi} + \frac{\partial F_i}{\partial \eta} + \frac{\partial F_v}{\partial \eta}\right) \tag{7}$$

in which $\frac{\partial E_i}{\partial Q}$ and $\frac{\partial F_i}{\partial Q}$ are the inviscid flux Jacobians in the ξ- and η- directions respectively and $\frac{\partial F_v}{\partial Q}$ is the viscous flux Jacobian in the η-direction. The flux Jacobians are calculated using analytical expressions. Turbulent contributions to the flux Jacobian are neglected because of the difficulties posed in finding analytical expressions from the Baldwin-Lomax model which exhibit a sparse structure.

Equation (7) represents a sparse, system of linear equations of the form,

$$[A]\{x\} = \{b\} \tag{8}$$

which can be solved using conjugate gradient methods. In this work restarted GMRES [20] is employed. The system of equations represented by Equation (8) is generally ill-conditioned which has severe consequences for the convergence of conjugate gradient methods.

In order to improve the condition of the system matrix, and hence the convergence behaviour of the linear solver, preconditioning is required. We seek a preconditioning matrix which when used to pre-multiply Equation (8) results in a new system of linear equations,

$$[C][A]\{x\}=[C]\{b\} \tag{9}$$

which is more amenable to solution by iterative techniques. The pre-conditioner used in this work is based upon ADI factorisation. Badcock and Richards [21] have demonstrated that such an approach provides a fast and effective pre-conditioner for the two-dimensional Navier-Stokes equations.

Results

The method described in the proceeding sections has been applied to the calculation of steady and unsteady flows for several aerofoils. In order to help establish confidence in the present numerical method the results of steady state computations for the RAE 2822 aerofoil are presented. The ability of the method to predict unsteady flows is demonstrated by comparison of calculated results with experimental measurements for the unsteady flow around a NACA 0012 aerofoil undergoing both inplane and pitching oscillations. Finally calculations of the unsteady flowfield around a NACA 0012 aerofoil undergoing combined translation-pitch oscillations are presented.

Steady flow around RAE 2822 aerofoil

Steady state calculations were performed for the RAE 2822 aerofoil at a Mach number of 0.73, a Reynolds number of 6.5 million and an angle of attack of 2.79 degrees in order to establish the overall accuracy of the numerical method. Calculations were performed on a relatively coarse grid having 159 grid points in the streamwise direction (100 on the aerofoil surface) and 48 grid points in the normal direction. Calculated pressure distributions are compared with the

experimental data of Cook et al[22] in Figure (1). The computations show good agreement with experiment over the entire aerofoil, although the location of the shock wave is slightly downstream of that observed in the wind tunnel tests. The calculated lift coefficient of 0.791 is in fair agreement with the experimental value of 0.803.

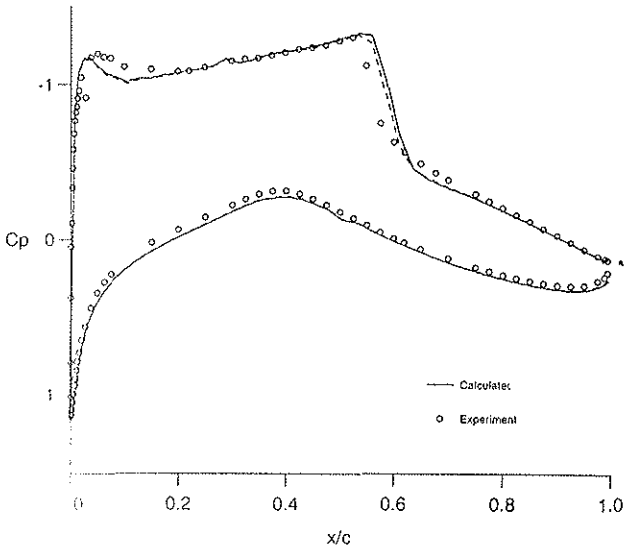

Figure (1) RAE 2822 Aerofoil:
$\alpha = 2.79^{\circ}, M_{\infty} = 0.73, Re_c = 6.5$ **million.**

NACA 0012 aerofoil with in-plane motions

The normal component of Mach number for a rotor blade section located a distance r from the axis of rotation is given by,

$$M_{\infty} = \frac{r}{R} M_{tip}(1 + \mu^{*} \sin(\psi)) \qquad (12)$$

in which R is the radius of the rotor blade, M_{tip} is the tip Mach number in hover, μ^{*} is the ratio of forward flight speed to the rotational velocity, i.e. $\mu^{*} = \frac{U_f}{\frac{r}{R}U_{tip}}$, and ψ is the azimuth angle. Neglecting three dimensional effects Equation (12) provides a basis for calculating the aerodynamics of helicopter rotor blades using the in-plane motions of aerofoils. Under this approximation the rotational speed of the rotor blade provides a mean flow Mach number, $\frac{r}{R}M_{tip}$, while the forward flight Mach number can be represented by a grid velocity term,

$$\frac{dx}{dt} = \frac{r}{R} M_{tip} \mu^{*} \sin(k^{*} t) \qquad (13)$$

here, $\mu^{*} = \frac{R}{r}\mu$ and the non-dimensional frequency, k^{*}, is obtained from,

$$k^{*} = \frac{\omega c_{local}}{u_o} = \frac{\omega c_{local}}{\omega r} = \frac{c_{local}}{r} \qquad (14)$$

Unsteady flow calculations have been performed for the NACA 0012 aerofoil on a fine grid containing 251 nodes in the streamwise direction (200 on the aerofoil surface) and 96 nodes in the aerofoil direction, see Figure (2). In the remainder of this section results are presented for inplane oscillations described by,

$$M_{\infty} = 0.5113, \mu^{*} = 0.5263, k^{*} = 0.1976$$

These conditions represent the flow at $\frac{r}{R} = 0.84$ on the rotor blade tested by Tauber et al[23] at a hover tip Mach number of 0.598 and an advance ratio of 0.45.

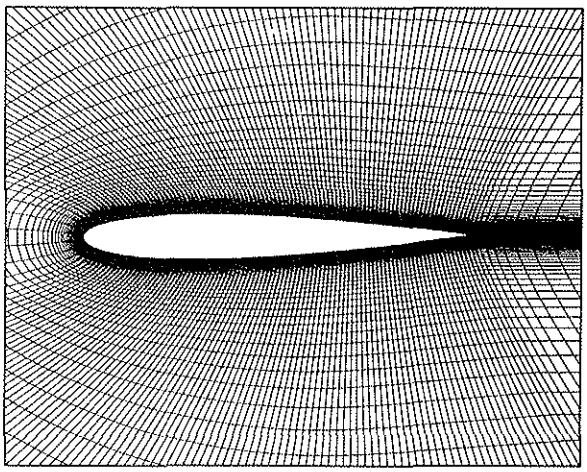

Figure (2) Detail of the Fine (251x96) Computational grid for NACA 0012 aerofoil.

Figure (3) shows the development of the unsteady pressure distribution over the advancing side of the rotor disc, additionally results at azimuth angles of 30, 60, 90, 120 and 150 degrees are shown in Figure (4). At low azimuth angles the calculated flowfield is dominated by a rapid expansion of the flow at the leading edge, this is a characteristic feature of the relatively blunt NACA 0012 aerofoil. As the free stream Mach number increases with increasing azimuth angle a region of high pressure gradient develops towards the trailing edge, this region grows in extent until eventually shock waves form on the aerofoil surface close to the mid-chord point. The shock waves then migrate towards the trailing edge growing in strength. The maximum Mach number is achieved at 90 degrees azimuth while the maximum shock strength is obtained at an azimuth angle slightly beyond 90 degrees as the flow begins to decelerate. As the flow decelerates further the shock waves move back towards the aerofoil mid-chord point decreasing in strength before finally disappearing.

The importance of dynamic effects can be demonstrated by comparing unsteady pressure distributions at symmetric azimuth angles, i.e. azimuth angles which have the same instantaneous Mach number. For instance, comparing Figures 4(b) and 4(d) we observe dramatic differences, without and with a shock wave respectively. The influence of flow unsteadiness is further demonstrated when unsteady results are compared with steady calculations performed for the same instantaneous Mach number. In Figure (5) such a comparison is made for azimuth angles of 60 and 120 degrees. From this Figure we see that for the unsteady flow shock strength is reduced when compared with the steady solution, while for decelerating flow dynamic effects are unfavourable.

The flow physics which were expected have been reproduced qualitatively by the unsteady calculations. No corresponding experimental data has been found in the open literature and consequently the physical accuracy of the current method cannot be properly demonstrated. Instead comparison is made between the calculated two dimensional results and experimental data obtained by Tauber et al[23] in helicopter rotor tests. Agreement between calculated and measured pressure distributions is generally good for cases in which there is no strong shock wave, see for example Figures 4(a),(b) and (c). At 90 degrees azimuth, Figure 4(c), the calculated shock wave appears to be moderately weaker than that observed in the experiment and is slightly downstream of the experimentally determined position. Results at 120 degrees azimuth, Figure 4(d), compare poorly with experiment upstream of the shock wave. The calculated shock wave is more than 10% of the chord length aft of that recorded in the experiment and is of much greater strength.

In order to investigate the numerical accuracy of the results calculations were performed to determine the influence of time step and grid resolution. It was found that the current time step (corresponding to 0.25 degrees azimuth per iteration) was acceptable. Comparison of calculations performed on the fine grid and a coarser grid containing 153x48 grid points show small differences, see Figure (4), which are associated with improvements in resolving the shock wave more accurately.

NACA 0012 aerofoil with pitching motion

The ability of the present numerical method to predict the unsteady flowfields of aerofoils performing pitching oscillations has been investigated. In the present paper unsteady calculations are presented for AGARD test case 5[24]. For this test case a NACA 0012 aerofoil is pitched harmonically about the quarter chord axis at a free stream Mach number of 0.755. The oscillatory motion is described by,

$$\alpha = \alpha_0 - \Delta\alpha \sin(k\tau) \qquad (15)$$

in which $\alpha_0 = 0.016$ degrees is the mean angle of attack, $\Delta\alpha = 2.51$ degrees is the amplitude of the oscillation and k=0.0814 is the reduced frequency based upon semi-chord. No artificial transition mechanism was utilised during the experiments, consequently calculations were performed with a fully turbulent boundary layer.

The development of the unsteady flowfield with time is shown in Figure (8). The flow can be characterised by the periodic appearance and disappearance of shock waves on the upper and lower surfaces. Initially, at low incidences, weak shock waves exist on both the upper and lower surfaces. As the angle of attack is increased the upper surface shock wave increases in strength, while that on the lower surface diminishes before finally disappearing. The shock wave on the upper surface continues to increase in strength and migrates towards the mid-chord position as the incidence is increased further. After the maximum incidence is achieved the shock wave on the upper surface begins to diminish in strength and move back towards the leading edge position. On the lower surface a region of high pressure gradient develops over the aft region of the aerofoil chord. As the angle of attack is reduced further this region grows in extent until finally a shock wave is formed close to the 30% chord position. The upper and lower surface shock waves move in opposite directions, towards and away from the leading edge respectively, with decreasing incidence. The computed flowfield has been found to be almost symmetric, this can be demonstrated by close inspection of the curve of calculated normal force coefficient presented in Figure (6), and consequently the flow behaviour observed over the first half of the aerofoil motion is repeated in the second half of the cycle.

Calculated normal force and pitching moment coefficients are compared with experimental measurements in Figures (6) and (7). While the comparison between calculation and experiment is good for low angles of attack and during the upstroke agreement during the down stroke is disappointing. The differences observed between calculation and experiment for normal and pitching moment coefficients are also evident when the calculated pressure distributions are compared with experiment, see Figure (8). In general the comparison with experiment is favourable. During the up stroke both shock position and shock strength are well predicted while for the down stroke the shock is stronger and further forward than observed in the experiments.

It should be noted that while the calculations show the expected symmetry between the first and second halves

of the cycle (symmetry is expected due to the low amplitudes of the motion and proximity of the mean incidence to zero) the experiment does not. There are several possible explanations for this apparent discrepancy. Firstly in the current calculations both the low amplitude, higher harmonic content of the unsteady incidence and the low amplitude Mach number oscillations observed by Landon[23] have been ignored. Of perhaps even greater importance is that the experimental data has not been corrected for unsteady wind tunnel interference effects, it is likely therefore that both the mean angle of incidence and the amplitude of the motion used in the current calculation do not truly reflect the behaviour of the model in the wind tunnel experiment.

Combined translation-pitch oscillations

While the aerodynamics of aerofoils performing inplane and pitching oscillations provides physical insight into the behaviour of the flowfield it must be remembered that the true motion of the rotor aerofoil in forward flight is composed of simultaneous inplane and pitching oscillations. A more complete model of the unsteady aerodynamics of helicopter rotor aerodynamics must therefore include coupling of the two rigid body motions. In the remainder of this paper the behaviour of a NACA 0012 aerofoil subjected to combined translation-pitch oscillations is investigated. Calculations have been performed for aerofoil motions described by the equations,

$$M = M_{Tip}(1 + \mu^* \sin(k^* \tau)) \qquad (16)$$

$$\alpha = \alpha_0 - \Delta\alpha \sin(k^* \tau)$$

with the following flow conditions:

$$M_\infty = 0.5113 \, , \mu^* = 0.5263$$

$$k^* = 0.1976$$

$$\alpha_0 = 0.016 \text{ and } \Delta\alpha = 2.51 \, .$$

Note that the Mach number and incidence variations match those of the inplane and pitching moments presented above.

Instantaneous pressure distributions and Mach number contours obtained for the second cycle of the unsteady calculation are displayed in Figures (9) and (10) respectively, while in Figure (11) the unsteady lift coefficient is plotted. For the purposes of Figure (10) the local Mach number is measured with respect to the moving grid, this frame of reference has the advantage that regions of 'forward' and 'reverse' flow relative to the aerofoil are easily identifiable.

Initially the flowfield is found to be almost symmetric, Figure 10(a), and no shock waves are evident. For low azimuth angles the pressure distributions and variation of normal force indicate that the development of the flow is dominated by changes in angle of attack. As the free stream Mach number nears the critical value appreciable pressure gradients develop on both the upper and lower surfaces of the aerofoil. The pressure gradient grows most rapidly on the lower surface and it is here that the shock wave forms. The growing importance of variations in Mach number as the aerofoil enters the transonic regime are emphasised by the delay in the formation of the shock wave beyond the (steady flow) critical Mach number. This delay in shock formation is attributed to the favourable dynamic effects of accelerating flow seen previously for inplane oscillations alone. Further evidence of the importance of Mach number related dynamic effects is seen in the behaviour of normal force coefficient which appears to decrease more rapidly for higher Mach numbers. By an azimuth angle of around 60 degrees a weak shock wave has formed on the lower surface close to the mid-chord point, this shock wave grows in strength as the incidence and free stream Mach number increase further and moves gradually towards the trailing edge, as the azimuth angle approaches 90 degrees a small degree of trailing edge separation flow separation becomes apparent in the solution. The boundary layer is observed to thicken as the shock strength increases.

At an azimuth angle of 90 degrees the maximum Mach number (M_∞=0.78) and minimum angle of incidence (α=-2.494) are attained, at these conditions a small separation bubble is formed at the foot of the shock wave. The shock wave continues to move slightly downstream and increase in strength until the separation bubble extends from its foot to the trailing edge, this behaviour is reflected by a small plateau in the normal force coefficient. Once the flow downstream of the shock wave separates fully from the aerofoil surface the nature of the shock-boundary layer interaction changes. For further increases in azimuth angle the shock-boundary layer interaction is much stronger and this is reflected in the increasingly oblique angle which the shock wave forms to the aerofoil surface.

As the azimuth angle increases further we observe that the shock wave moves towards the leading edge and reduces in strength while the free shear layer, which is clearly evident in the Mach number contour plots, moves away from the aerofoil surface. The movement of the free shear layer ultimately leads to the formation of a stall vortex, rotating in an anti-clockwise direction, close to the lower surface of the aerofoil. The presence of this vortex is clearly evident in the pressure distributions for azimuth angles in the range 110 to 140

degrees. The stall vortex travels towards the trailing edge of the aerofoil. Close to the trailing edge secondary separation is observed forward of the primary vortex . This region of recirculating flow quickly becomes separated from the aerofoil surface and travels with the primary vortex towards the trailing edge. The vortices have been shed into the wake by an azimuth angle of 155 degrees. The development and shedding of the stall and secondary vortices causes large fluctuations in the normal force (and also pitching moment) coefficient, which changes from approximately -0.4 to 0.3 very rapidly as the vortices form and then reduces again as the vortices move along the aerofoil and are shed into the wake.

Following the shedding of the vortex, and final disappearance of the shock wave, the boundary layer becomes fully attached once more. Unsteady effects for azimuth angles corresponding to the retreating blade are weak, this is reflected by the small level of hysterisis observed it the normal force coefficient for positive angles of attack.

Separated flow was not observed for pitching and translation oscillations alone. This creates some difficulties when relating the aerodynamics of the isolated motions with those of the combined motion for which boundary layer separation did occur. It is clear however from the present calculations that the unsteady flow development is dominated by variations in Mach number while the flow is transonic, this conclusion is reached because of evidence for the delay of both shock formation beyond the (steady) critical Mach number and large scale flow separation, which is not observed until Mach number begins to decrease. At azimuth angles for which the flow is subsonic and fully attached the flow development appears to be dominated by changes of incidence. Only weak unsteady effects are evident for retreating side azimuth angles where the Mach number is small. This finding is consistent with the findings of a number of authors, see for example Lerat[1], who have found similar behaviour for aerofoils performing low amplitude pitching oscillations at constant velocity in incompressible flow.

Conclusions

A method has been presented for the solution of the Reynolds averaged thin layer Navier-Stokes equations for aerofoils performing inplane and pitching aerofoils. The method has been used to study the aerodynamics of aerofoils performing isolated pitch and translation oscillations. Fair agreement is observed when the calculated results are compared with experiment. The present method was also applied to the calculation of the flowfield about a NACA 0012 aerofoil performing a combined pitch-translation oscillation representative of the motion performed by helicopter rotor aerofoils.

Calculations for the combined motion indicate flow separation over a wide range of azimuth angles from approximately 90 - 150 degrees azimuth. This feature was not observed in calculations for the individual motions and clearly illustrates the need to consider interactions between the two rigid body motions when designing aerofoils for high performance helicopter applications.

The relative importune of the dynamic effects due to changing Mach number and incidence has also been demonstrated. It seems clear from the present calculations that the unsteady flow development is dominated by variations in Mach number while the flow is transonic, this conclusion is reached because of evidence for the delay of shock formation beyond the (steady) critical Mach number and the promotion of large scale flow separation which is not observed until Mach number begins to decrease. At azimuth angles for which the flow is subsonic and fully attached the flow development appears to be dominated by changes of incidence. Only weak unsteady effects are evident for retreating side azimuth angles where the Mach number is small.

The Baldwin-Lomax turbulence model is generally acknowledged to produce poor estimates of turbulent viscosity for large scale separation due to difficulties in determining a suitable length scale. In addition the model contains no mechanism for including historical information about turbulence. In view of these remarks the use of such a model in the present work casts some doubt over the quantitative results obtained for the combined motion. In order to obtain a more physically valid representation of turbulence work is currently underway to implement more modern turbulence models for the present problem.

Acknowledgements

This work is funded by EPSRC under contract number GR/K31664. The authors would like to thank Professor B. Richards and Dr K. Badcock of Glasgow University and Dr. A. Kokkalis and Mr R. Harrison of Westland Helicopters Ltd for their invaluable assistance.

References

1. Maresca, C., Favier, D. and Rebont, J. Experiments on an aerofoil at high angle of incidence in longitudinal oscillations, J. Fluid Mech., 1979, 92, pp 671-690.
2. Gursul, I. and Ho, C. High aerodynamic loads on an airfoil submerged in an unsteady free stream, AIAA J., April 1992, 30, (4), pp 1117-18.
3. Shih, C. and Ho, C. Vorticity balance and time scales of a two dimensional airfoil in an unsteady free stream, Phys. Fluids, February 1994, 6, (2), pp 710-23.

4. Gursul, I., Lin, H. and Ho, C. Effects of times scales on lift of airfoils in an unsteady free stream, AIAA J., April 1994, 32, (4), pp 797-801.
5. Gursul, I., Lin, H. and Ho, C. Parametric effects on lift force of an airfoil in unsteady free stream, AIAA J., May 1996, 34, (5), pp 1085-87.
6. Krause, E. and Sweitzer, W.B. The effect of an oscillatory free stream-flow on a NACA -4412 profile at large relative amplitudes and low Reynolds numbers, Experiments in Fluids, 1990, 9, pp 159-166.
7. Morinishi, K. and Muratu, S. Numerical solutions of unsteady oscillating flows past an airfoil, AIAA 92-3212, July 1992.
8. Lerat, A. and Sides, J., Numerical simulation of unsteady transonic flows using the Euler equations in integral form, ONERA TP-79-10, February 1979.
9. Habibie, I., Laschka, B. and Weishaupl, C., Analysis of unsteady flows around wing profiles at longitudinal accelerations, ICAS 94, 1994.
10. Lin, C.Q. and Pahlke, K., Numerical solution of Euler equations for aerofoils in arbitrary unsteady motion, Aeronaut J., June 1994.
11. Shaw S.T. and Qin, N. Solution of the Navier-Stokes equations for the flow around an aerofoil in an oscillating free stream, ICAS 1996.
12. Gaitonde, A. L., A dual time method for the solution of the unsteady Euler equations, Aeronaut J., October 1994, pp 283-91.
13. Badcock, K. J., Computation of turbulent pitching aerofoil flows, University of Glasgow, Aero Report 9322, 1993.
14. Richter, R. and Leyland, P., Precise pitching airfoil computations by use of dynamic unstructured meshes, AIAA 93-2971, July 1993.
15. Paraschivoiu, M., Unsteady Euler solution for oscillatory airfoil and oscillating flap, AIAA 92-0131, January 1992.
16. Favier, D., Agnes, A., Barbi, C., and Maresca, C., Combined translation/pitch motion: A new airfoil dynamic stall simulation, Journal of Aircraft, Vol. 25, No. 9, September 1988.
17. Favier, D., Belleudy, J., Maresca, C., Influence of coupling incidence and velocity variations on the airfoil dynamic stall, 48th American Helicopter Society Forum, Washington, June 1992.
18. Van der Wall, B.G. and Leischman, J.G., Influence of variable flow velocity on unsteady airfoil, 18th European Rotorcraft Forum, September 1992.
19. Favier, D., Berton, E., Pascazio, M., Wang, C.M., Tullahoma, T. and Steinhoff, J.S., Experimental and numerical investigation of airfoil dynamic stall in combined pitch-translation oscillation, AIAA 95-0310, January 1995.
20. Saad, Y., and Schultz, M.H., GMRES: A generalised minimum residual algorithm for solving non-symmetric linear systems, SIAM J. Sci. Stat. Comp., 7, (3), 1986.
21. Badcock, K.J. and Richards, B.R., Implicit methods for the Navier-Stokes Equations, AIAA J., March 1996.
22. Cook, P., McDonald, M., and Firmin, M., Aerofoil RAE 2822 - Pressure distribution and boundary layer wake measurements, AGARD R-138, 1979.
23. Tauber, M.E., Chang, I.C., Caughey, D.A. and Phillipe, J.J., Comparison of calculated and measured pressures on straight and swept tip model rotor blades, NASA TM 85872, December 1983.
24. Landon, R.H., NACA 0012 Oscillatory and transient pitching, Section 3, AGARD Report 702, August 1982.

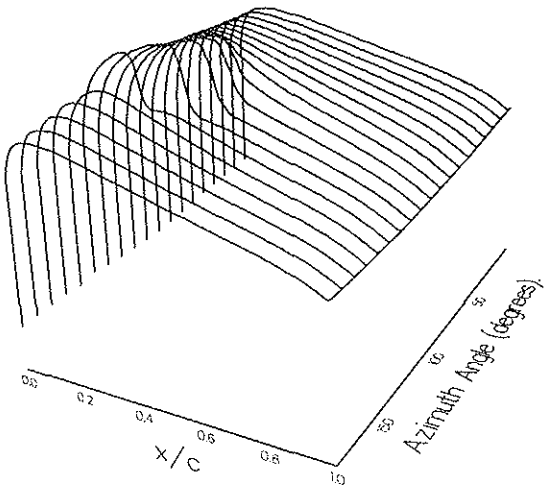

Figure (3) Development of advancing side pressure distribution for inplane oscillations.

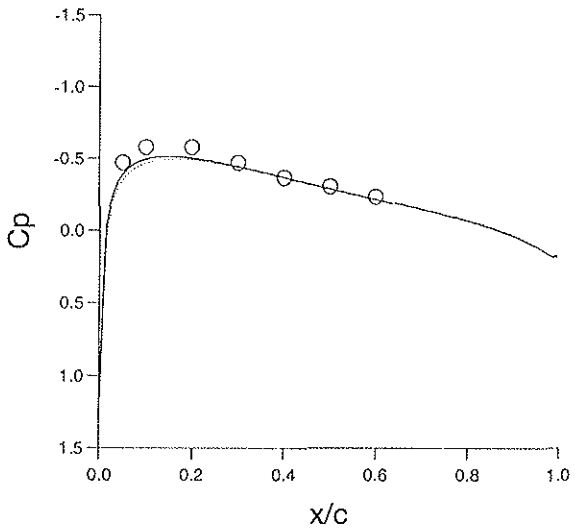

(4a) ψ = 30 degrees.

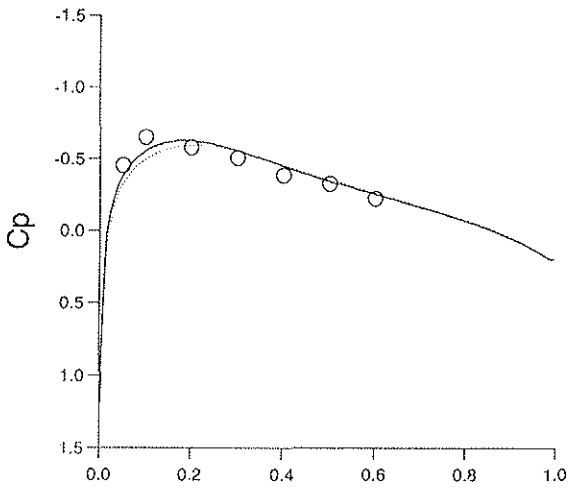

(4b) ψ = 60 degrees.

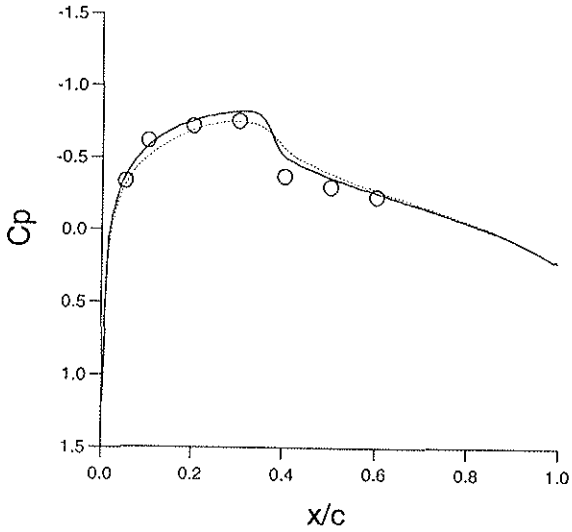

(4c) ψ = 90 degrees.

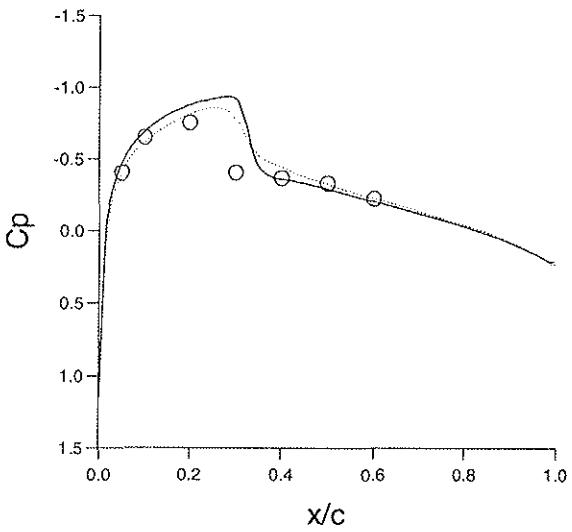

(4d) ψ = 120 degrees.

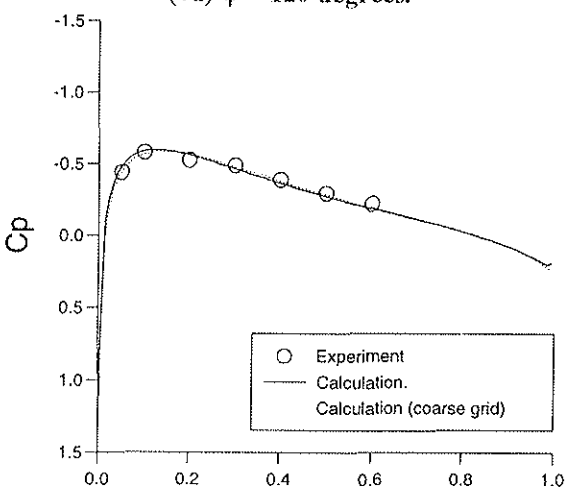

(4e) ψ = 150 degrees.

Figure (4) Comparison of calculated and measured pressures for inplane oscillations.

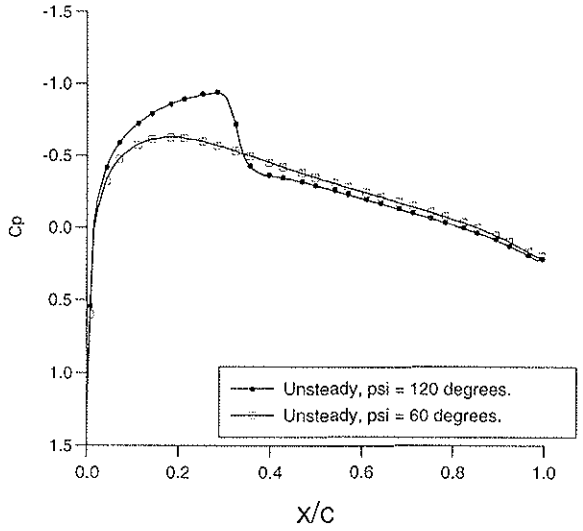

Figure (5) Comparison of unsteady pressure coefficients at symmetric azimuth angles.

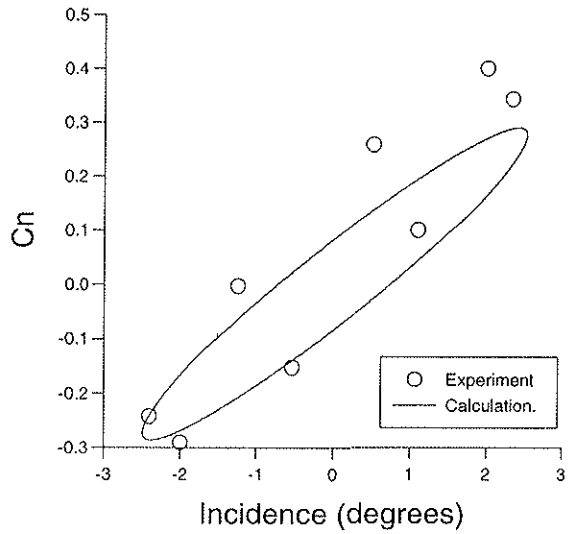

Figure (6) Comparison of computed and measured normal force coefficients for pitching oscillations.

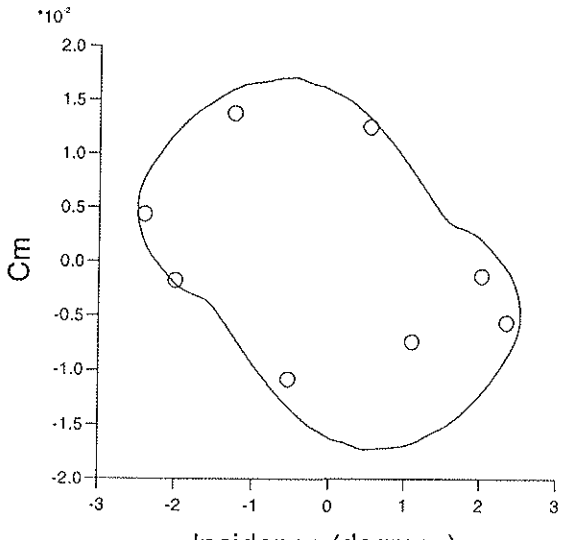

Figure (7) Comparison of computed and measured pitching moment for pitching oscillations.

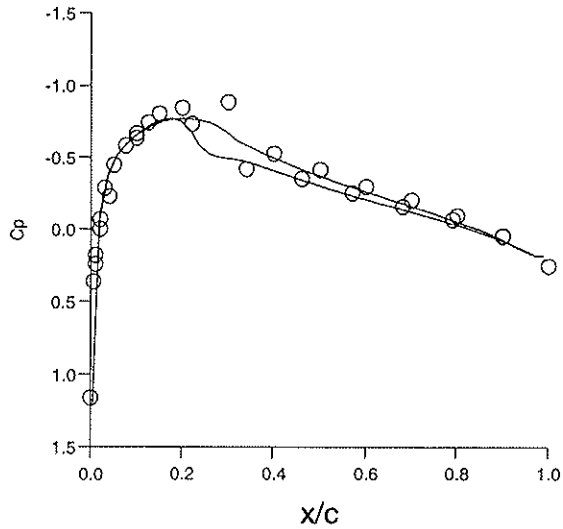

(8a) α = 1.09 degrees.

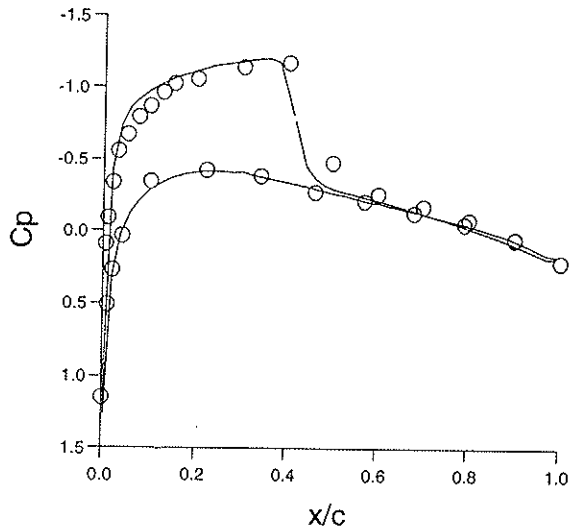

(8b) α = 2.34 degrees.

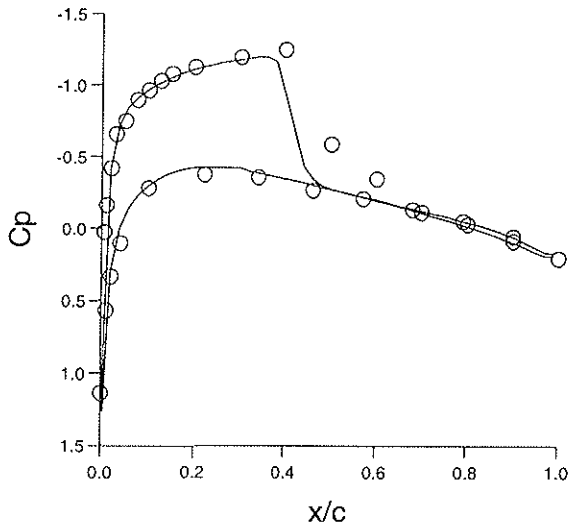

(8c) α = 2.01 degrees.

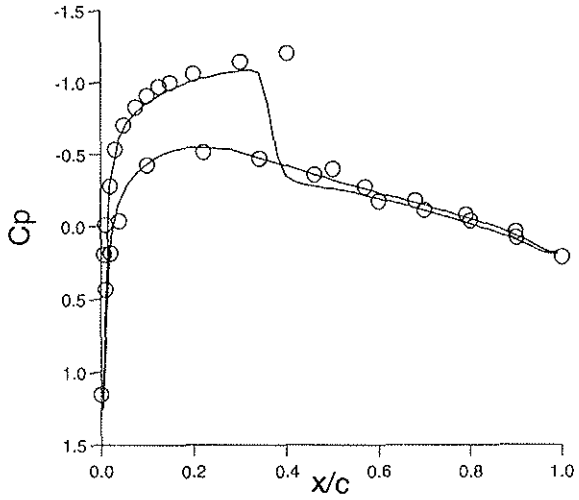

(8d) α = 0.52 degrees.

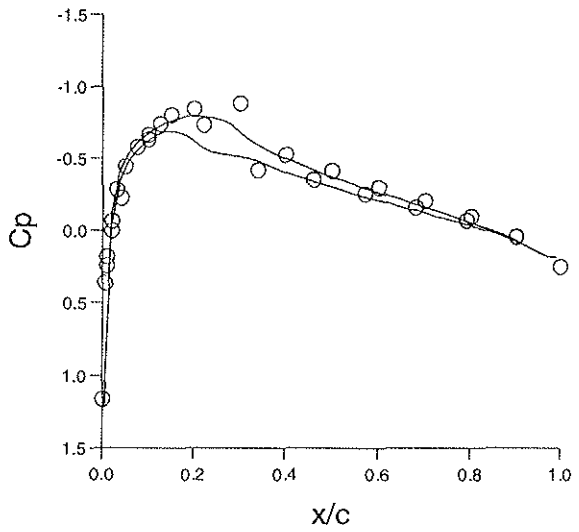

(8e) α = -1.25 degrees.

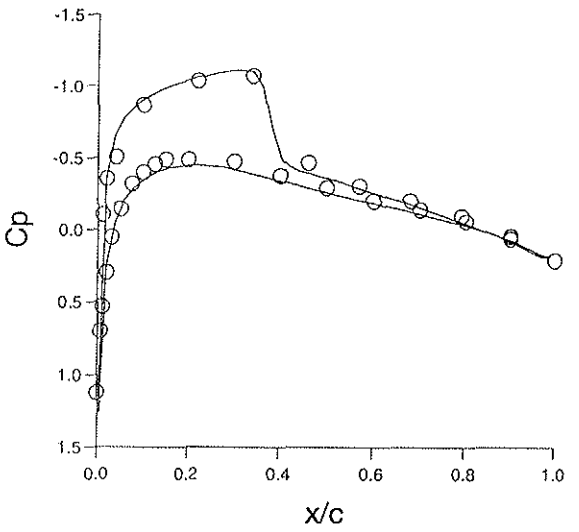

(8f) α = -2.41 degrees.

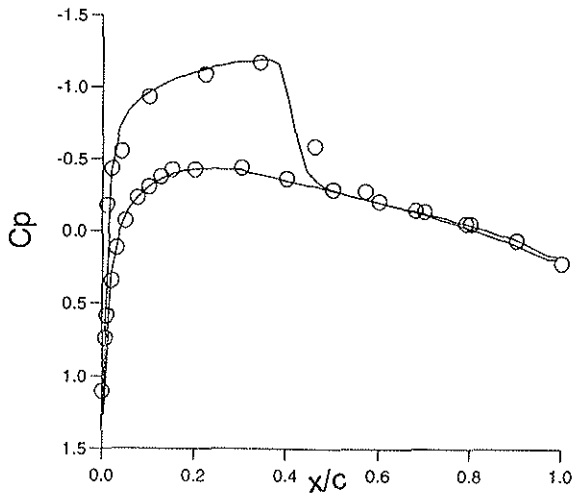

(8g) α = -2.00 degrees.

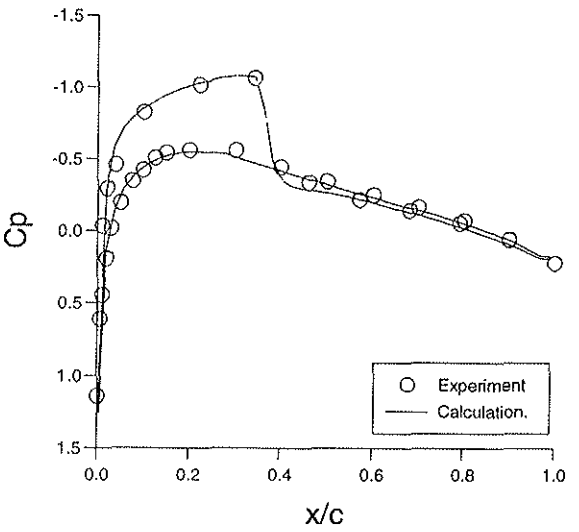

(8h) α =-0.54 degrees.

Figure (8) Comparison of measured and calculated pressures for pitching oscillations.

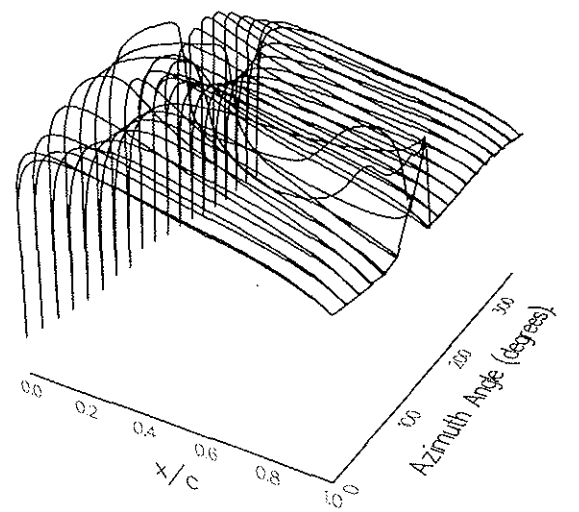

Figure (9) Calculated pressures for combined translation-pitch oscillation.

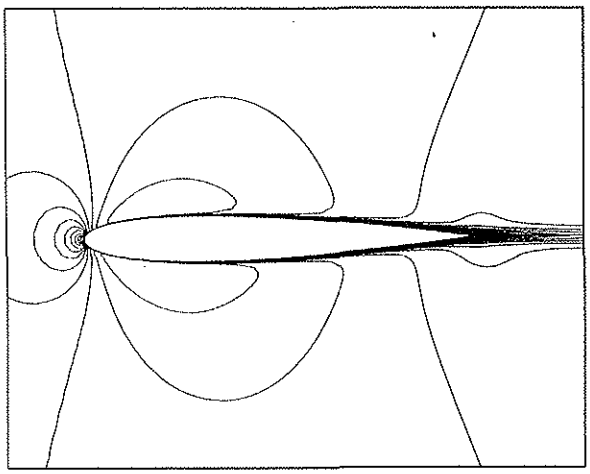

Figure (10a) ψ = 10 degrees.

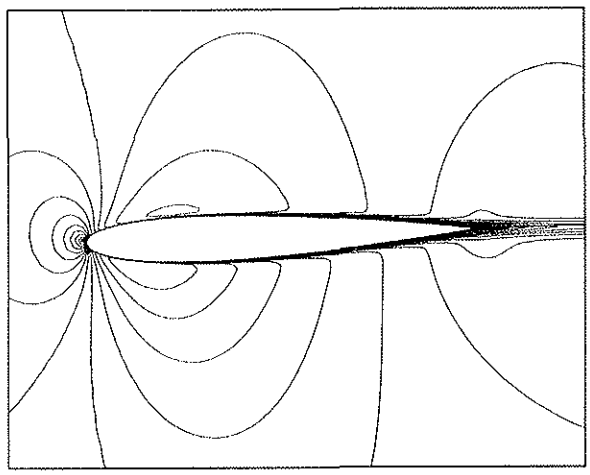

Figure (10b) ψ = 50 degrees.

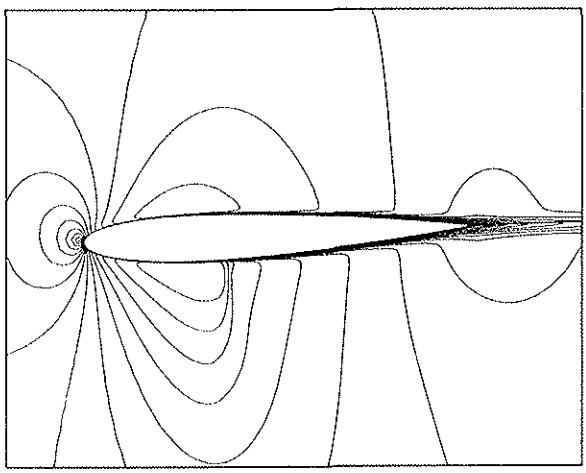

Figure (10c) ψ = 70 degrees.

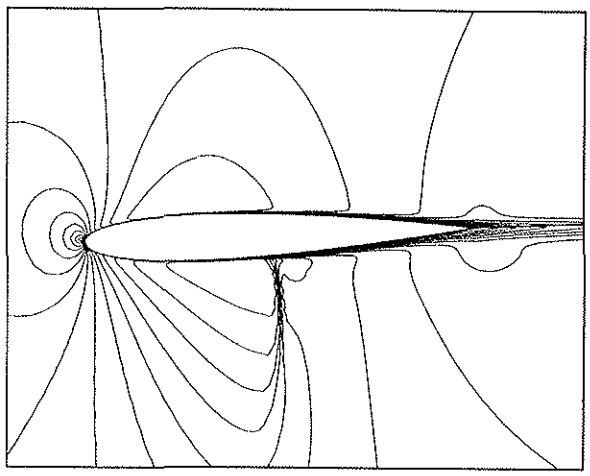

Figure (10d) ψ = 85 degrees.

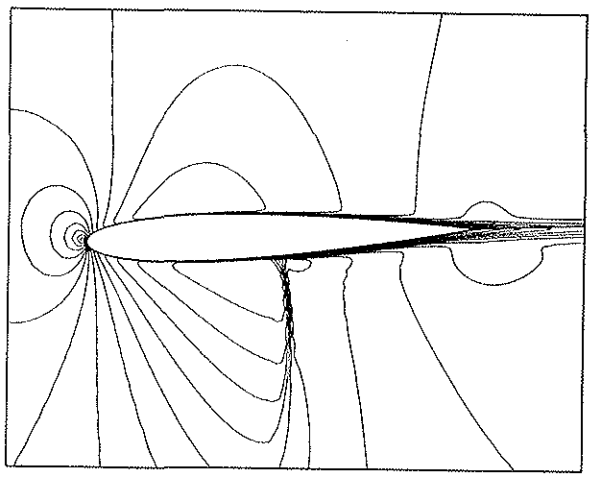

Figure (10e) ψ = 90 degrees.

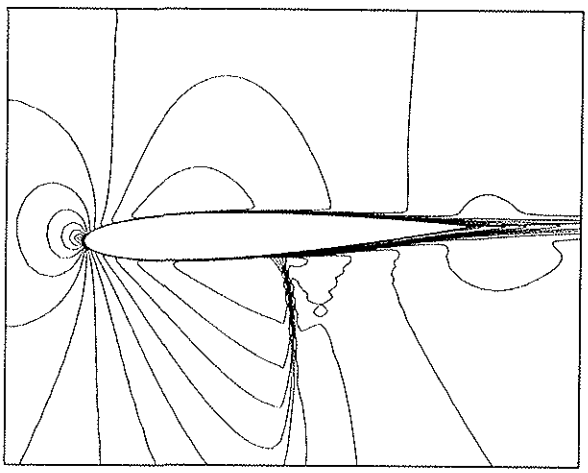

Figure (10f) ψ = 95 degrees.

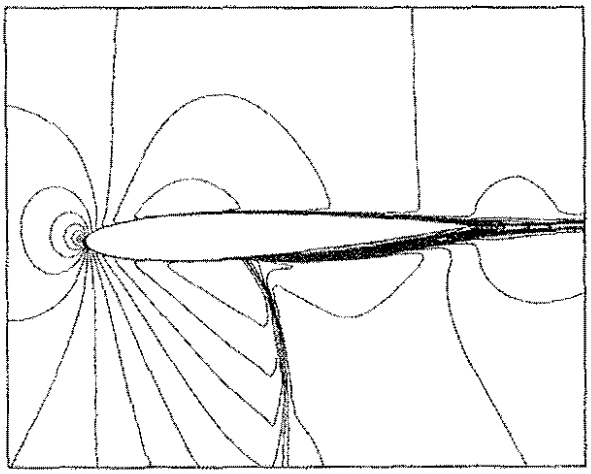

Figure (10g) ψ = 110 degrees.

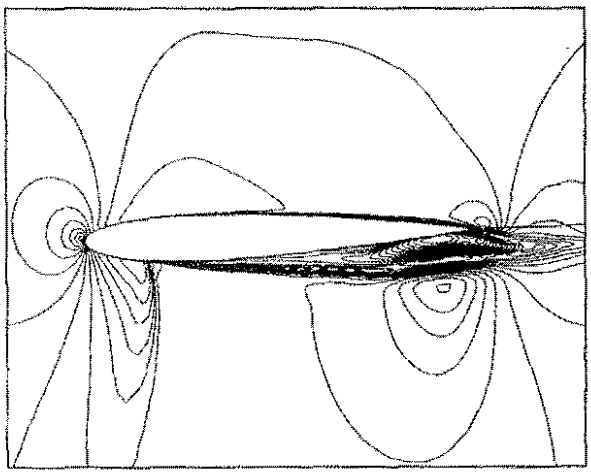

Figure (10j) ψ = 130 degrees.

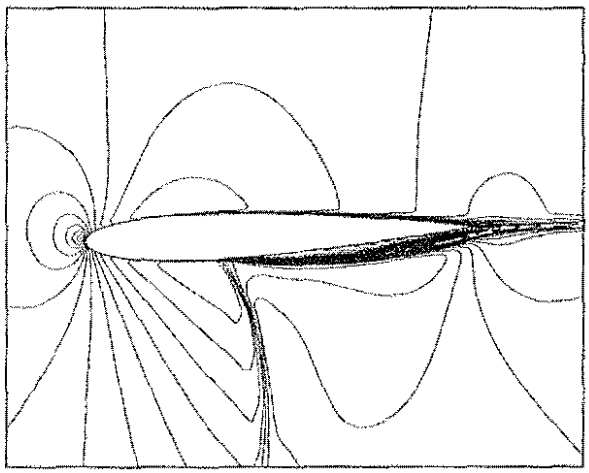

Figure (10h) ψ = 115 degrees.

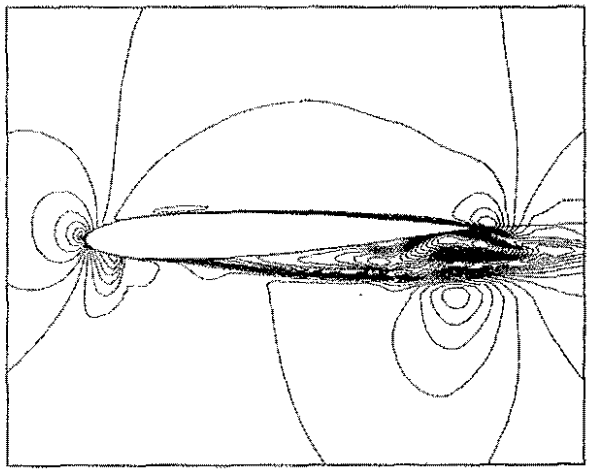

Figure (10k) ψ = 135 degrees.

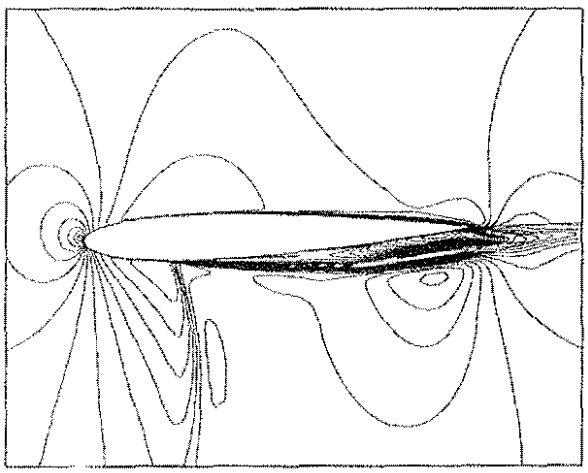

Figure (10i) ψ = 125 degrees.

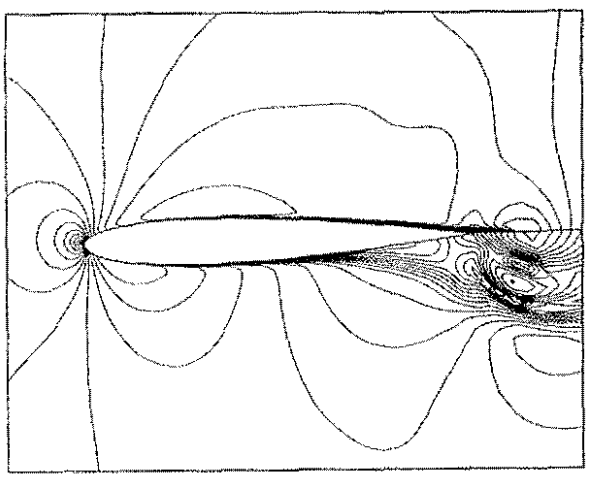

Figure (10l) ψ = 145 degrees.

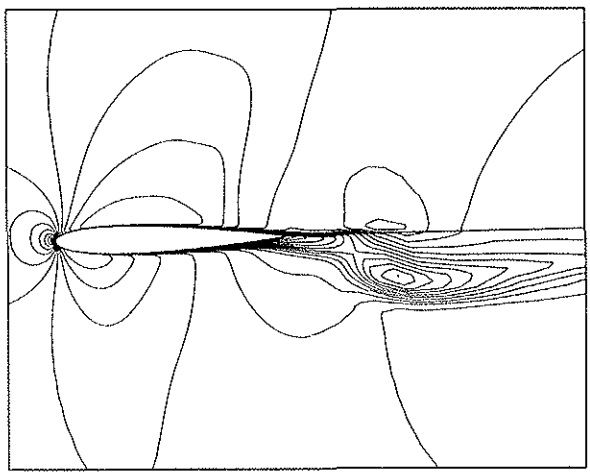

Figure (10m) ψ = 150 degrees.

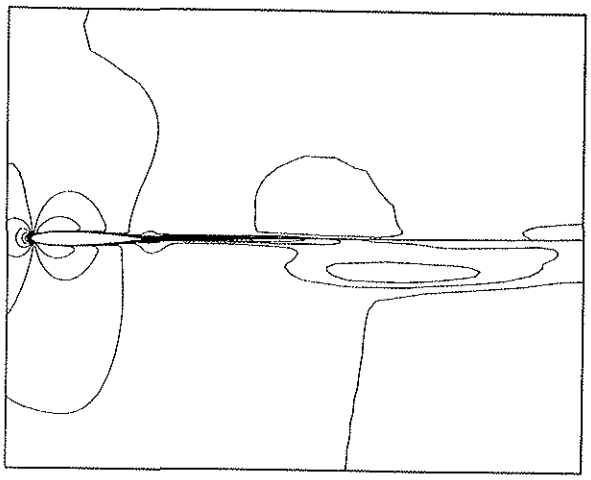

Figure (10p) ψ = 170 degrees.

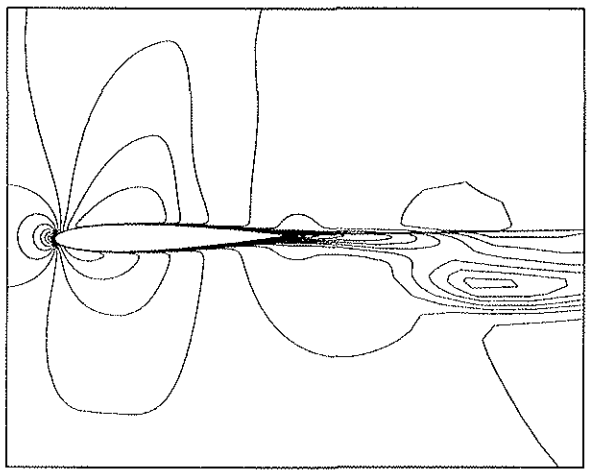

Figure (10n) ψ = 155 degrees.

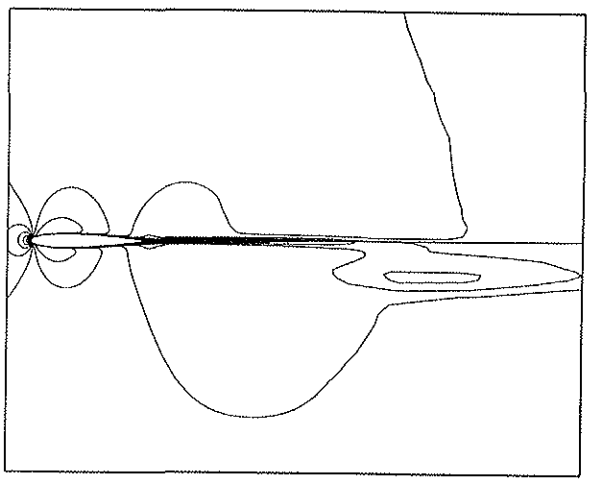

Figure (10q) ψ = 175 degrees.

Figure (10) Instantaneous Mach number contours.

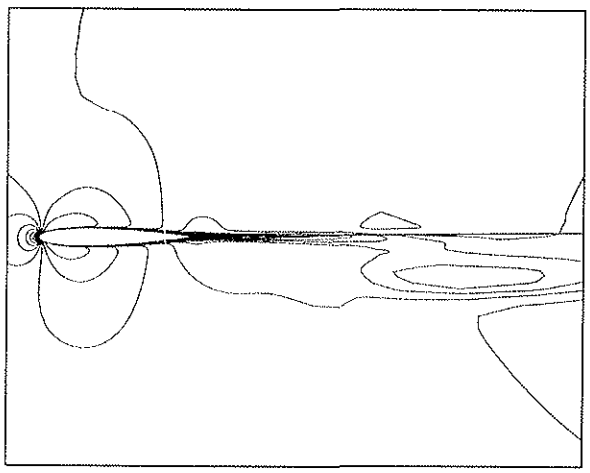

Figure (10o) ψ = 165 degrees.

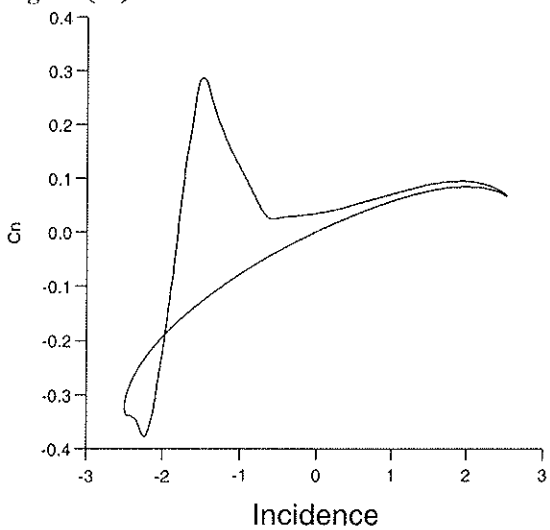

Figure (11) Calculated normal force coefficient.